Journal of Materials Chemistry B

Accepted Manuscript

ROYAL SOCIETY OF CHEMISTRY

www.rsc.org/materialsB

In vitro evaluation of biodegradable magnesium alloys containing micro-alloying additions of strontium, with and without zinc

Junlan Wang[*1], Shayanti Mukherjee[*2], David R. Nisbet[2], Nick Birbilis[1], Xiaobo Chen[1#]

[1]Department of Materials Science and Engineering, Monash University, Clayton, Victoria 3800, Australia
[2]Research School of Engineering, The Australian National University, Acton, ACT 0200, Australia

[*] Equal Contribution
[#] Corresponding Author (xiaobo.chen@monash.edu)

Abstract: The *in vitro* degradation of magnesium (Mg) alloys containing low levels of strontium (Sr, 0.05, 0.1 and 0.2 wt.%) with and without additions of zinc (Zn, 0.5 and 1.0 wt.%), was studied for potential use in orthopaedic fracture treatments. Sr-containing Mg-alloys were selected as a promising strategy to utilise the biological role of Sr through alloying, to induce accelerated bone tissue growth. The influence of controlled alloying upon degradation rate was studied via electrochemical measurements and immersion tests in minimum essential medium (MEM). Immersion testing revealed a comparable degradation rate of the alloys tested herein, indicating no detrimental effect of Sr on degradation. Cytotoxicity experiments on primary mouse osteoblasts indicated good biocompatibility and enhanced proliferation of osteoblasts for all the tested Mg alloys. Potentiodynamic polarisation testing further confirmed that low-level additions of Sr imparted a minor influence on cathodic kinetics, with a slight inhibition of anodic kinetics. In contrast, the addition of Zn as a ternary element moderated both anodic and cathodic kinetics of Mg-Sr alloys.

Keywords: Magnesium, Strontium, Biomaterials, Orthopaedics, MEM, Cytotoxicity.

1. Introduction

Magnesium (Mg) alloys are emerging biomaterials for orthopaedic applications owing to their desired mechanical and biological features.[1-5] In addition, the *in vivo* degradation of Mg alloys minimises inflammatory and allergic responses through forming non-toxic oxides / hydroxides, and more importantly, eliminates secondary surgery to remove invasive implants after bone fractures have been fully healed.[3, 6] The surgical success of the implantation of Mg devices depends greatly on a controllable degradation process, which suppress adverse hydrogen gas evolution (the cathodic reaction which accompanies Mg dissolution), deterioration of mechanical strength, and dramatic changes in local pH in the chloride-rich physiological environments.[3, 7] Alloying Mg exemplifies an effective method to address the degradation issue through altering its microstructure, mechanical properties and electrochemistry.[6, 8]

It has been well documented that calcium (Ca) and zinc (Zn) elements are the most commonly explored alloying elements for Mg alloy implants.[9, 10] Addition of Ca into Mg matrix gives rise to brittle and anodic Mg_2Ca intermetallic phases existing along grain boundaries, which significantly deteriorates ductility and adversely accelerates degradation of the resulting alloys.[9, 11-13] The presence of excessive Zn and Mg-Zn based precipitates, may lead to accelerated and uneven degradation in the physiological environments due to the formation of numerous micro-galvanic couples in the alloy microstructure. In contrast, strontium (Sr), another critical trace element in the human body (with 99 wt.% of Sr stored in bone), has been confirmed to stimulate bone tissue growth and inhibit bone resorption through its modulation of bone cell recruitment and function, even being orally administrated to treat osteoporosis.[14-16] In addition, it has been shown that alloying Mg with Sr of an appropriate quantity, varying between 0.5 - 5 wt. %, can improve its mechanical strength to some extent.[17-19] As such, introducing Sr into the Mg matrix provides a new pathway towards development

of Mg implants with sufficient strength, satisfactory degradation, accelerated bone tissue growth and strong implant-bone fixation, for shorter recovery duration and alleviated cost and pain for the patient.

Prior studies of relevance to the development of Mg-Sr(-Zn/Ca/Zr) based biomaterials, have mainly focused on the role of Sr in regulating corrosion and mechanical properties (in the context of structural alloys, not in the bio-environment or bio-context), and/or biocompatibility, with Sr concentration varying between 0.5 - 5 wt. %, far beyond the 0.11 wt. % solubility limit of Sr in Mg.[18, 20-22] Herein, we explored biodegradable Mg alloys containing micro-levels of Sr as promising implant candidates, which are of paramount importance in terms of orthopaedic applications, but have been scarcely reported to date. The beneficial bone-tissue stimulating effect of Sr warrants significant further attention as functional and valuable additions to degradable Mg implants that are intended to dissolve at the rate of bone growth.

The rational of the compositions and experiments studied herein stems from:

(a) The limited maximum daily allowance of Sr (approximate 5 mg per day per adult by oral administration).[14]

(b) The low solid (metallurgical) solubility of Sr in Mg (approximately 0.11 wt.%) results in the tendency to form Sr-containing intermetallics that dramatically increase its dissolution rates. Ideally, a homogeneous microstructure that dissolves *uniformly* is desired.

(c) Alloying with low levels of Sr (as an exclusive biological regulator) into Mg alloy systems provides a strategy in the development of new biodegradable implants that accelerate bone growth owing to the biological function of Sr, *with minimum adverse impact on the original mechanical properties and degradation rate*.

In this study, we explored custom binary Mg-Sr alloys with Sr contents well below previously reported compositions, at 0.05, 0.1 and 0.2 wt.%, respectively, along with ternary Mg-Sr-Zn alloys with the addition of Zn, in an attempt to mitigate the likely accelerated degradation progress of the binary Mg-Sr alloys.[19] Microstructure and phase chemistry of various Mg-Sr(-Zn) alloys were characterised using scanning electron microscopy and X-ray diffraction. Biodegradation behaviours of the samples were evaluated through immersion testing over defined time durations and electrochemical analysis at physiological conditions in minimum essential medium (MEM). The effect of discrete alloying concentrations on biocompatibility was assessed by cytotoxicity study towards primary mouse osteoblasts exposed to biodegradation extracts with varying dilutions - aimed at elucidating the impact of low levels of Sr on biodegradation, mechanical and preliminary cytotoxic properties of Mg-Sr(-Zn) alloys.

2. Materials and Methods

2.1 Sample preparation

Mg alloys were synthesised by induction melting 99.9 wt.% pure Mg (≤ 40 ppm Fe) (AMAC, Australia) with either pure Zn (99.9%) (Alfa Aesar, USA) or Mg-31Sr (wt.%) master alloy (Alfa Aesar, USA), in a graphite coated steel crucible under the protection of an argon atmosphere. The pure Mg before alloying was stored in cool, dry wooden boxes, whilst the alloy samples after fabrication were stored in vacuum desiccators to avoid contamination and oxidation (corrosion). To avoid oxidation and ignition of molten Mg, the furnace chamber was evacuated down to ~10^{-2} bar and filled with argon gas. All apparatus that contacted with the molten Mg, including stirrer, thermocouple protector and mould, were coated with graphite to minimise Fe contamination. The mixture of metals was heated up to 720 °C at a rate of 3 - 5 °C s^{-1} and maintained for 25 - 30 min, with vigorous stirring every 5 min. The melt was then poured into a rectangular mould preheated to 200 °C to reduce shrinkage, followed by cooling down to room temperature at an average rate of 1 °C s^{-1}. The nominal and analysed chemical compositions of the alloy samples, determined by inductively coupled plasma atomic emission spectrometry (ICP-AES) (Spectrometer services), are listed in **Table 1**. Mg with commercial purity of 99.9 wt.% (≤ 40 ppm Fe) was also used as a control.

2.2 Microstructural characterisation

Scanning electron microscopy (SEM) was conducted using a JEOL 7001F equipped with a Bruker energy dispersive X-ray spectroscopy (EDX) system. Specimens were grounded progressively down to 2000 grit finish with silicon carbide paper, followed by polishing with 3 and 1 μm diamond paste prior to final polishing with 0.5 μm colloidal silica suspension to obtain a mirror-like finish. The polished specimens were then chemically etched using a picric acid solution to reveal the grain boundaries.

Phase analysis of the as-cast alloys was conducted using X-ray diffraction (Philips PW1140) under the condition of CuKα radiation (λ = 1.5418 Å), 40 kV and 25 mA at a scanning speed of 0.5 °C min^{-1} between 10 - 80°.

2.3 Immersion testing

Alloy samples were cut into cubes of 5 mm in each dimension and prepared to a 2000 grit SiC paper finish for mass loss testing, performed in minimum essential medium (MEM, Invitrogen) in a sterile Sanyo incubator at constant temperature of 37 °C in a humidified atmosphere containing 5% CO_2. The chemical compositions of MEM and human plasma are compared in **Table 2**.[27] The samples were ultrasonically cleaned in ethanol in for 3 min prior to immersion in MEM. A constant ratio of volume of MEM to sample area of 150 ml cm^{-2} was employed to minimise the influence of pH and ionic strength variation.[23] pH value was 7.4 at the beginning of immersion and the MEM solution was refreshed every 2 days to maintain the ion concentrations (and bulk pH). After immersion for 1, 3, 7 and 14 days, respectively, samples were removed from MEM solution and cleaned using 200 g l^{-1} of chromic acid and 10 g l^{-1} $AgNO_3$ for 1 min according to the ASTM G1-03 standards to remove corrosion products, followed by drying in air.[24] The weight of each specimen was carefully measured before and after immersion to determine a mass loss / degradation rate over different time durations of immersion. The mass loss was recorded as degradation rate in a unit of mg day^{-1} cm^{-2} and mean values were obtained from triplicate experiments.

2.4 Electrochemical measurements

Electrochemical tests were performed using a flat cell (EL-FLAT_3, Bio-Logic®) containing 250 ml MEM medium at 37 °C and pH 7.4 ± 0.4. The cell has a double jacket for temperature control and three holes for reference electrode, purge tube and temperature probe. The potentiodynamic polarisation tests were carried out at a scan rate of 1 mV s^{-1} after 10 min open circuit potential (OCP)

conditioning. The corrosion current density i_{corr} and corrosion potential E_{corr} were estimated by linear fitting the polarisation curves using EC-Lab software (version 10.39, BioLogic®). The polarisation curves provide kinetics of anodic and cathodic reactions of the tested samples, which can be applied to interpret their corrosion mechanisms. A minimum of five replicates were taken for each specimen for reproducibility.

2.5 Primary osteoblasts isolation and identification

Primary osteoblasts were isolated from femur bone of adult Swiss mice according to Australian National University animal ethics guidelines. The femur bone was cleaned thoroughly, minced and digested using collagenase (Sigma-Aldrich) at a concentration of 10 mg ml^{-1} at 37 °C for 20 min. The digested mass was washed with 1 × Phosphate Buffer Saline (PBS) and plated on tissue culture plate (TCP) and maintained with Dulbecco's modified Eagle's DMEM (Thermo Fisher Scientific) containing 20% fetal bovine serum, FBS (Gibco), and 1% penicillin- streptomycin antibiotics (Thermo Fisher Scientific) in incubators at 37 °C in a humidified atmosphere containing 5% CO_2. Confluent cultures were mechanically detached using cell scrapers (Thermo Fisher Scientific) and seeded at a density of 10,000 cells per sample in 24 well plates. Isolated primary bone cells grown on samples were washed with PBS, and fixed with 4% paraformaldehyde (Sigma-Aldrich) for 10 min. Cells were permeabilised with 0.1% Triton X-100, blocked for non-specific staining using 3% BSA and then immunostained with Phalloidin-TRITC (Millipore) and anti-osteocalcin antibody (R&D systems) for 1 h at room temperature and then, revealed with anti-species-specific Alexa fluor 488 (Life Technologies). The samples were mounted using anti-quenching mounting medium (Vectashiled, Vector laboratories) and observed under for the fluorescence images (IX 71, Olympus).

2.6 Isolation and characterisation of primary mouse osteoblasts

To validate that cells isolated from femur bone of mice are able to differentiate into various lineages, we cultured the isolated primary mouse osteoblasts on tissue culture plates (TCP) and carried out immunochemical stains to characterise the various linages observed. Images of the isolated cells on TCP display a mixed population of cells. The cells with a small shape were designated to characteristic fibroblast-shaped osteoblasts and osteoclasts whilst the larger cells with greater cytoplasmic area were osteocytes after cultured for 7 days and 14 days (**Fig. 1**a and **1**b). Osteoblasts and osteoclasts are bone cells that are responsible for synthesizing and resorbing bone tissue, respectively. It is also apparent that the cell density increased with culture time. The characterised staining (**Fig. 1**c, **1**d and **1**e) demonstrates the expression of two proteins synthesised by the osteoblasts: F-actin and osteocalcin, which indicates that the isolated cells consisted primarily of osteoblasts. F-actin is mainly involved in crucial cellular processes like morphogenesis, cell division, and migration, and osteocalcin is expressed only by osteoblasts.[25]

2.7 Preparation of alloy extracts

Three samples of each alloy were cut into cubes of 5 mm in length and ground to a 2000 grit using SiC paper. The samples were ultrasonically cleaned in ethanol for 15 min and sterilised under UV light for 1 h before being placed in 1 ml of DMEM without FBS at 37 ºC in incubators filled with humidified air containing 5% CO_2. Alloy extracts were prepared by removal of alloys after two scheduled durations of 2 and 10 h. Since Mg corrodes at high rates during the initial post-implantation (immersion) time frames, which incurs severe concerns on biocompatibility, we chose 2 h and 10 h immersion to get extracts for indirect analysis. This method has been adopted extensively in many published works, in which long-term immersion was performed to evaluate degradation behaviours of Mg alloys but short-term (i.e. 2, 6, 10 up to 15 h) immersion extracts were collected to evaluate cytotoxicity specifically.[26-

[29] The extracts were then centrifuged at 500 × g for 5 min and the supernatants were collected, following by reconstituting into 10, 1 and 0.1% when incubated primary bone cells. The weight of each specimen was carefully measured before and after immersion to determine mass loss at different time intervals. The ion concentrations were calculated by mass loss according to their corrosion reactions.[27]

2.8 Cytotoxicity tests

Cell proliferation in alloy extracts was determined using the colorimetric Vybrant MTT Proliferation assay kit as per manufacturer's protocols (Life Technologies) at 3 day and 7 day time points. For the assay, cells were rinsed with PBS to remove unattached cells and incubated with 10% MTT reagent in a serum free medium for a period of 3 h at 37 °C and 5% CO_2 incubators. Absorbance of the obtained dye was measured at 490 nm using a spectrophotometric plate reader (TECAN Infinite® 200 PRO series).

2.9 Statistical analysis

Statistical analysis was conducted with Origin 9.5. Significant differences were determined using one-way ANOVA followed by Tukey's test. The experimental results are reported as mean ± SD (standard deviation), and p values < 0.05 were considered statistically significant.

3. Results

3.1 Microstructural characterisation

XRD analysis (**Fig. 2**) illustrates all the major peaks of the binary Mg-Sr and ternary Mg-Zn-Sr alloys were identified as a single phase of α-Mg matrix, i.e. Sr is integrated into the solid solution with a characteristic hexagonal close packed (hcp) structure, signalling no detectable presence of $Mg_{17}Sr_2$ intermetallic phases and/or unalloyed Sr/Zn phases. Though, on a theoretical basis, $Mg_{17}Sr_2$ intermetallic precipitates should exist in the case of Mg-0.2Sr alloy in which the Sr addition was slightly larger than 0.11 wt.%, the volume fraction is likely too low to be ascertained. Backscatted electron (BSE) mode images and EDX mapping (**Fig. 3**), on the contrary, reveal visible secondary particles dispersed within the Mg matrix, and the density of intermetallic particles of ternary Mg-1Zn-0.1Sr (*ca*. 2450 mm^{-2}) is half of that in binary Mg-0.1Sr alloy (*ca*. 4720 mm^{-2}). The density of intermetallic particles increases as a function of Sr content in binary Mg-Sr alloys, which is evident from the BSE images of Mg-0.05Sr (*ca.* 3541 mm^{-2}), Mg-0.1Sr (*ca.* 4718 mm^{-2}) and Mg-0.2Sr (*ca.* 8678 mm^{-2}) in **Fig. 2**. According to the equilibrium phase diagram of Mg-Sr alloys, the intermetallic precipitates should be designated to be $Mg_{17}Sr_2$ phase.[30]

3.2 Immersion testing

The degradation rates of Mg alloys were displayed in the form of mass loss after immersion in MEM over 1, 3, 7 and 14 days (**Fig. 4)**. The degradation rate increases with immersion time from the onset stage to the intermediate immersion stage, i.e. 7 days, independent of chemical composition and microstructure of the alloys. The difference in degradation rate of discrete sample groups is not statistically significant, demonstrating a marginal influence of addition of Sr (≤ 0.2 wt.%) with and without Zn. Specifically, within the initial 24 h timeframe, the degradation progress proceeds relatively

slowly, with a value varying from 0.6 - 0.8 mg day^{-1} cm^{-2}, whilst the degradation rate rises progressively up to 1.2 - 1.6 and 2.0 - 2.2 mg day^{-1} cm^{-2} after immersion for 3 and 7 days, respectively. However, the longest immersion procedure, i.e. 14 days, gave rise to a significant change in the degradation behaviour of the sample groups. In brief, pure Mg continued dissolving into MEM (2.3 mg day^{-1} cm^{-2}), ternary Mg-1Zn-0.1Sr alloy had a suppressed corrosion development (1.7 mg day^{-1} cm^{-2}), whilst the other alloys exhibited a constant degradation process (varying from 2.0 to 2.1 mg day^{-1} cm^{-2}).

Fig. 5 illustrates surface morphology of the representative binary Mg-0.1Sr and ternary Mg-1Zn-0.05Sr alloys after immersion in MEM for 24 h, given the similarity in the corroded morphology of all tested alloys. In general, the original metallic finish disappeared and a thick coating containing numerous profound cracks was present over the entire surface. EDX analysis on the selected regions (1 and 4) as indicated in **Fig. 5**a and **5**b, confirms that the newly formed coating comprising corrosion products was made up from Ca and P, two essential components of MEM, implying characteristic localised/heterogeneous corrosion undergoing with the immersion in MEM. Similar results were reported in prior study that immersion of Mg-0.5Sr into SBF formed a stable layer of calcium phosphate compounds covering its surface.[20] Such deep cracks may facilitate aggressive attacks from corrosive medium towards the underneath metals. The relatively smooth regions with less cracks (region 2 in **Fig. 5**a) are rich in Mg and O instead, which is attributed to the formation of $MgO/Mg(OH)_2$ passive layer in contact with aqueous solution. Sr was not detected due to the trace amount of Sr below the probing resolution of EDX, though a small amount of Zn was detected in ternary Mg-1Zn-0.05Sr alloy (**Fig. 5**b).

3.3 Electrochemical analysis

Fig. 6 presents the potentiodynamic polarisation curves of pure Mg, binary Mg-Sr and ternary Mg-Zn-Sr alloys in MEM at 37 °C. To explore the role of Sr in regulating corrosion kinetics of binary Mg-Sr alloys, a comparison of polarisation curves was depicted (**Fig. 6**a), which reveals the anodic kinetics of Mg were inhibited as a function of addition of Sr. The corresponding cathodic branches were unaltered by the addition of Sr. In contrast, addition of Zn into the Mg-Sr alloy system induced a notable retardation of both the anodic and cathodic kinetics (**Fig. 6**b and **6**c). According to **Table 3,** pure Mg had a slightly higher corrosion current density of 32.5 ± 2.6 μA cm^{-2} than that of binary Mg-Sr alloys (21.0 ± 1.8 μA cm^{-2}), irrespective of the quantity of added Sr, whilst ternary Mg-Sr-Zn displayed a notably lower corrosion current density of about 8.7 ± 1.6 μA cm^{-2} than that of pure Mg and Mg-Sr alloys, exhibiting a passivating role of Zn in terms of corrosion of Mg-Sr alloy system.

3.4 Evaluation of cellular proliferation of primary mouse osteoblasts in various extracts

According to the established protocols to measure cell viability, Mg alloy samples were placed in cell culture media with persistent dynamic shaking over two well-defined time durations, 2 h and 10 h, respectively, to accelerate degradation.[26, 27] Thereafter, a series of dilution of the supernatant of the media hosting the precedent alloy degradation at 0.1%, 1% and 10% (refer to **Table 4** for the original ion concentrations of Mg, Sr and Zn in the extracts prior to diluting process) were extracted and added into the primary mouse osteoblast culture (**Fig. 7)**. As 10% variability in inorganic ions has a negligible influence on human mesenchymal stem cells (hMCSs), it is logical to deduce that primary mouse osteoblast herein can tolerate 10% change in inorganic ions as well.[31] As such, differences of cellular proliferation were owing to additional Mg, Sr and Zn ions in the media. Cell proliferation, presented by normalised increase or decrease in cell density compared to media control, was analysed by MTT assay after culture over 3 days and 7 days, respectively. It is noteworthy that cell proliferation was promoted

in all diluted concentrations of the alloying extracts that collected after 2 h and 10 h immersion. In addition, a similar increasing trend in cell density demonstrates that both the dilution ratio (i.e. 0.1%, 1% and 10%) and immersion timeframe of Mg alloys in DMEM (2 h and 10 h) have a marginal impact on cell proliferating behaviour.

4. Discussion

4.1 Influence of micro-level additions of Sr on the biodegradation behaviours of Mg with and without Zn in MEM

The microstructure of the binary Mg-Sr alloys (**Fig. 3**) reveals visible $Mg_{17}Sr_2$ particles within the Mg matrix, and the density of these secondary particles increases with the nominal quantity of the added Sr. This can be attributed to the extremely low solid solubility of Sr in Mg (*ca*. 0.11 wt.% at 585ºC), where excess Sr will be rapidly enriched in the liquid phase and gives rise to precipitation in the form of $Mg_{17}Sr_2$ intermetallic phase during solidification.[30] In the case of ternary Mg-Zn-Sr alloys, it is noteworthy that the number density of the identified $Mg_{17}Sr_2$ particles in Mg-1Zn-0.1Sr (*ca*. 2454 mm^{-2}) is half of that in Mg-0.1Sr alloy (*ca*. 4718 mm^{-2}), indicating that addition of Zn (≤ 1.0 wt.%) reduces segregation of Sr in Mg as previously reported by Xia et. al.[19] Moreover, the high solid solubility of Zn with respect to Mg (6.2 wt.%) leads to homogeneous distribution of Zn in Mg matrix, without any detectable segregation (**Figs. 2** and **3**).[10] The hardness measurement by Xia et al. also confirmed that addition of micro-level Sr slightly increased the hardness of Mg alloys by solid solution hardening.[19]

The correlation between addition of Sr, with and without Zn in Mg and their degradation performance in MEM was explored through mass loss testing (**Fig. 4**).[32] In general, pure Mg and Mg alloys containing micro additions of Sr, irrespective of the presence of Zn, display comparable degradation behaviour at each defined time duration, except for 14 days that indicates a lower degradation rate for Mg-1Zn-0.1Sr than that of the other sample groups. This indicates that the presence of Sr exhibited no detrimental effect on corrosion performance of Mg in MEM, provided the additions were well controlled around the solubility limit. It merits comment that this differs from results which indicate that the same micro levels of Sr lead to severe deterioration of corrosion

resistance when studied as structural alloy, the case of a differing environment of unbuffered 0.1 M NaCl at ambient temperature.[19] This discrepancy can however be ascribed to the discrete chemical nature of the two electrolytes, i.e. 0.1 M NaCl and MEM, which notably have a significant influence on corrosion behaviour of Mg-Sr alloys. Mg alloys are prone to dissolution in electrolytes containing Cl^- anions (100 mM in 0.1 M NaCl and 123.5 mM in MEM). Dissolution is further enhanced in the presence of $Mg_{17}Sr_2$, owing to the micro-galvanic couples between the matrix and $Mg_{17}Sr_2$ that localise corrosion.[18] However, what we observe is that at physiological temperatures, and owing to the additional species in MEM (including Ca and phosphate ions), the present study confirmed the presence of Ca and phosphate in MEM greatly influences, favourably, the anticipated degradation of Mg-Sr alloys. In other words, the formation of a surface film containing Ca and P components that play a protective role (more so than the $Mg(OH)_2$ formed in 0.1 M NaCl alone) aide in mitigating corrosion on Mg alloy surface (**Fig. 5**).[20-22, 33, 34] Such so called deficient-'apatite' like films upon Mg in MEM have been previously noted by Waterman et al.[35] The findings herein, regarding the minimal influence of Sr on the overall degradation of Mg in MEM from micro-additions of Sr, is of particular importance for the design of new Mg alloy systems for implantable uses where only the biological function of Sr is being sought. In addition, the enhanced corrosion resistance of Mg-1Zn-0.1Sr alloys after immersion in MEM for 14 days may be attributed to the synergetic effect of Sr and Zn. A similar combined influence of low levels of Sr and Ca on Mg-related degradation has also been recently reported.[21]

It can be ascertained that the dissolution rates of all sample groups increased as a function of immersion time in MEM over the first 7 days, which is in contrast to some prior results.[32] A sound explanation is the relatively constant pH and ionic concentration in MEM that was refreshed every 2 days, along with a constant but large ratio of MEM volume to the surface area (i.e. 150 ml cm^{-2}) of the

samples in this study, whereas the simulated body fluid solutions were not replenished over the entire immersion periods in the prior study.[32] The sufficient replenishment of electrolyte is vital to retain the bulk pH from becoming alkaline (which results in decreased dissolution rates of Mg), and thus being closer to that of the real physiological environments, which may elucidate more realistic biodegradation behaviour of Mg alloys *in vivo*.

When immersion proceeded into the longer-term stage of the laboratory testing, i.e. between 7 to 14 days, it may reflect a surface condition where localised corrosion in MEM was no longer a dominant mode of dissolution, and any protective surface film became less sensitive to local pH. This led to gradual stabilisation of degradation rates (**Fig. 4**). In comparison, 24 h immersion gave rise to the surfaces of the representative samples (**Fig. 5**) containing both localised corrosion sites and CaP related degradation products, which indicates localised corrosion and CaP compounds on corrosion sites.[20] As corrosion proceeded, the accumulation of CaP compounds was elevated owning to the supplements from refreshed media. Upon the local phosphate concentration exceeded a threshold where phosphate was able to inhibit hydrogen evolution at focal sites, localised corrosion was no longer a principal attacking mode.[36]

Comparing the potentiodynamic polarisation curve of pure Mg with those of binary Mg-Sr alloys (**Fig. 6**a) reveals that micro additions of Sr exhibited a negligible effect on cathodic reactions, which has not been reported elsewhere to date in the bio-context. Addition of low level Zn into Mg-Sr system moderated both anodic and cathodic kinetics, which can be ascribed to the formation of stable oxide films on alloy surface and a reduced density of $Mg_{17}Sr_2$ by incorporation of Zn into Mg-Sr alloys (**Fig. 3**), respectively.

4.2 Proliferation of primary mouse osteoblasts subjected to various alloying extracts

The cell proliferation results demonstrate that extracts of all investigated Mg alloys promoted the proliferation (growth) of primary mouse osteoblasts, which is illustrated by percentage increase in cell density (approximate 25%), compared to the media control (**Fig. 7**). It has been well-defined that the original inorganic components in diluted (below 10%) alloying extracts derived from MEM have a marginal influence on cell growth,[18, 21, 27, 33] as such the positive influence is attributed to the presence of alloying elements degraded from metallic Mg alloys immersed in MEM. Though no clear concentration limits of Mg^{2+}, Sr^{2+} and Zn^{2+} as a stimulus for cell growth have been documented yet, it is logical to conclude from the results herein that concentrations of Mg^{2+}, Sr^{2+} and Zn^{2+} within ranges of 1×10^{-5} - 3×10^{-3} M, 1×10^{-9} - 1×10^{-6} M and 2×10^{-8} - 7×10^{-6} M (**Table 4**), respectively, well aligned within the boundary to play a beneficial role in regulating cell growth. It is noteworthy that the presence of Zn^{2+} ions exhibited a slight influence on cell proliferation of different alloy extracts, which elucidates that additions of micro-levels of Zn in Mg are biocompatible.[28] When excessive Zn is introduced into physiological environments, its biological role in modulating cellular responses is significant.[37, 38]

As expected, Sr implemented a dominant function to facilitate the growth of osteoblasts, compared to the counterpart ions, which is ascribed to its positive effect on replication, differentiation and lifespan of osteoblasts through down-regulating both the mRNA and protein levels of osteoblast-induced signals for osteoclastogenesis.[16, 39, 40] Both HA cements and calcium polyphosphate scaffolds doped with Sr exhibited an enhanced osteogenesis in comparison to the Sr-free counterparts.[41, 42] Moreover, the beneficial effect of Sr on bone-formation is dose-dependent, which may be overturned into detrimental aspect by excessive Sr content.[41, 43] Qiu et al. demonstrated that incorporation of 1 mol.% Sr in calcium polyphosphate scaffolds increased cell viability and ALP activity of ROS17/2.8 cells whilst Sr concentrations higher than 20 mol.% suppressed cell viability and ALP activity.[43] In

particular, Gu et al.[18] proposed that Sr concentrations below 5×10^{-4} M enhanced cell proliferation and ALP activity, and Park et al. [44] also showed that low levels of Sr ions (approximate 1×10^{-6} M) released from Ti64/Sr increased differentiation of osteoblasts. As such, concentrations of Sr ions around 1×10^{-6} M display a beneficial effect on osteoblastic behaviours, which is in accordance with the present findings that micro levels of Sr (1×10^{-9} - 1×10^{-6} M in media) released from Mg alloys contributed to growth of primary mouse osteoblasts. In the case of Mg alloys containing higher concentrations of Sr, Li et al. proposed that Mg-1Zr-2Sr exhibited the highest cell viability ratio and lowest haemolysis ratio amongst binary Mg-Zr and ternary Mg-(1-5)Zr-(2-5)Sr alloys.[22] Furthermore, *in vivo* studies also demonstrated that this alloy was a more preferable candidate to elicit osseointegration.[45] In their studies, Mg-1Zr-2Sr showed the lowest corrosion rate amongst these alloys, indicating the lowest ion concentration of Sr, which illustrated that low concentrations of Sr was preferable for cell viability. This strongly demonstrates that alloying of micro levels of Sr in Mg implant is safe and favorable in terms of bone growth.

It can be seen that none of the alloys displayed a significant difference in cell proliferation with different dilution ratio (0.1%, 1% and 10%) or with different submersing timeframe (2 h and 10 h, **Fig. 7**). The impact of the extracts of alloys on cell proliferation highly depends on ion concentrations in extracts. However, when concentrations of ions varied within the ranges that are favourable for cell growth, similar effects of those extracts on cell proliferation are observed. This has also been reported by Schumacher et al. and Gu et al. that no significant difference in cell proliferation were seen at Sr concentrations varying from 0 to 1×10^{-3} M and 0 to 5×10^{-6} M, respectively.[34, 46] Comparing the cell growth in the alloy extracts over different time duration, i.e. 3 days and 7 days, no significant increase was observed, which indicates that no detrimental effect on cell proliferation was evolved from longer exposure of cells to extracts.[20, 33] This finding is similar to previous *in vitro* studies that the viability of

MC3T3-E1 and MG63 cells after 5 days' culture were not reduced in comparison to that over 3 days' culture in media containing Sr ions.[18, 33] The *in vivo* study conducted by Tian et al. illustrated that incorporation of low dose of Sr in porous calcium polyphase scaffolds exhibited larger new bone volumes in rabbits with respect to the Sr-free scaffolds over 16-week implantation.[42] As such, it is logical to deduce that low levels of Sr-doped Mg implants can sustainably promote osteoblasts growth over longer terms. Nevertheless, more *in vivo* investigation regarding the biological performance of micro levels of Sr in bone growth is required.

In addition, the cell proliferation of different alloy extracts shows a relatively constant value, which indicates that additions of proper concentrations of Sr and Zn in Mg have no negative effect on cell growth, as discussed in the precedent paragraphs. Whilst the increase in cell proliferation for Mg-0.5Zn-0.05Sr was not as good as that for other alloy counterparts (**Figs. 7**), an significant increase was still seen, compared to the media controls. A lower cell proliferation value of Mg-0.5Zn-0.05Sr may be ascribed to the less favourable ratios of ions to cells.[33]

Overall, the present electrochemical, immersion exposure, and *in vitro* cytotoxicity studies demonstrate that alloying micro levels of Sr in Mg matrix promotes cell growth without compromising degradation and biocompatibility of Mg alloys over short and intermediate term, i.e. 3 days and 7 days. It illustrates a new pathway to prepare degradable Mg alloy implants with micro-additions of Sr to execute its promising biological role with minimal alteration on any other properties or functionalities.

5. Conclusions

The ability to incorporate Sr into degradable Mg alloys in the orthopaedic context presents an evolution towards functional biomaterial design. In this work, the influence of Sr present at micro-levels with and without Zn in Mg alloys on the *in vitro* degradation behaviour and cytotoxicity were investigated. The immersion testing over defined time durations reveals that the presence of low levels of Sr in the vicinity of its metallurgical solid solubility limit value exhibits no detrimental influence on biodegradation rates of Mg in MEM. Potentiodynamic polarisation illustrates for the first time that alloying of micro levels of Sr (0.05, 0.1 and 0.2 wt.%) do not promote the *in vitro* cathodic reaction whilst slightly moderating anodic kinetic upon Mg in MEM. It also reveals that additions of Zn (0.5 and 1.0 wt.%, respectively) can be beneficial for suppressing *in vitro* degradation of Mg-Sr alloys by retardation of the both anodic and cathodic kinetics. *In vitro* cytotoxicity testing (0.1, 1 and 10%) presents an increase in proliferation of primary mouse osteoblasts in contact with allying extracts with different dilution ratios, compared with the media controls, indicating the adopted micro additions of Sr, around its solid solubility of 0.11 wt.% in Mg implant, were favourable for bone growth. The present study suggests that it is feasible to develop biodegradable Mg implant candidates for orthopedic applications containing micro levels of Sr to accelerate bone tissue growth during degradation, with minimal impact on degradation behaviour.

Acknowledgements

This research was financially supported by the Australian Research Council (Discovery Project DP130103131) and National Health and Medical Research Council (Career Development Fellowship APP1050684). We gratefully acknowledge Xiaojian Xia for technical assistance with sample preparation. Microscopy was carried out at the Monash Centre for Electron Microscopy. JLW is the recipient of a Monash Postgraduate Scholarship.

References

1. N. T. Kirkland, J. Lespagnol, N. Birbilis and M. Staiger, *Corrosion Science*, 2010, **52**, 287-291.
2. M. P. Staiger, A. M. Pietak, J. Huadmai and G. Dias, *Biomaterials*, 2006, **27**, 1728-1734.
3. F. Witte, V. Kaese, H. Haferkamp, E. Switzer, A. Meyer-Lindenberg, C. Wirth and H. Windhagen, *Biomaterials*, 2005, **26**, 3557-3563.
4. Y. Xin, T. Hu and P. Chu, *Acta biomaterialia*, 2011, **7**, 1452-1459.
5. S. Yoshizawa, A. Brown, A. Barchowsky and C. Sfeir, *Acta biomaterialia*, 2014, **10**, 2834-2842.
6. Y. Zheng, X. Gu and F. Witte, *Materials Science and Engineering: R: Reports*, 2014, **77**, 1-34.
7. F. Witte, J. Fischer, J. Nellesen, C. Vogt, J. Vogt, T. Donath and F. Beckmann, *Acta Biomaterialia*, 2010, **6**, 1792-1799.
8. Y. Ding, C. Wen, P. Hodgson and Y. Li, *Journal of Materials Chemistry B*, 2014, **2**, 1912-1933.
9. Z. Li, X. Gu, S. Lou and Y. Zheng, *Biomaterials*, 2008, **29**, 1329-1344.
10. S. Zhang, X. Zhang, C. Zhao, J. Li, Y. Song, C. Xie, H. Tao, Y. Zhang, Y. He and Y. Jiang, *Acta Biomaterialia*, 2010, **6**, 626-640.
11. N. T. Kirkland, N. Birbilis, J. Walker, T. Woodfield, G. J. Dias and M. P. Staiger, *Journal of Biomedical Materials Research Part B: Applied Biomaterials*, 2010, **95**, 91-100.
12. H. R. B. Rad, M. H. Idris, M. R. A. Kadir and S. Farahany, *Materials & Design*, 2012, **33**, 88-97.
13. F. Witte, N. Hort, C. Vogt, S. Cohen, K. U. Kainer, R. Willumeit and F. Feyerabend, *Current opinion in solid state and materials science*, 2008, **12**, 63-72.
14. S. Dahl, P. Allain, P. Marie, Y. Mauras, G. Boivin, P. Ammann, Y. Tsouderos, P. Delmas and C. Christiansen, *Bone*, 2001, **28**, 446-453.
15. P. Marie, P. Ammann, G. Boivin and C. Rey, *Calcified tissue international*, 2001, **69**, 121-129.
16. P. Marie, D. Felsenberg and M. Brandi, *Osteoporosis International*, 2011, **22**, 1659-1667.
17. K. Hirai, H. Somekawa, Y. Takigawa and K. Higashi, *Materials Science and Engineering: A*, 2005, **403**, 276-280.
18. X. Gu, X. Xie, N. Li, Y. Zheng and L. Qin, *Acta Biomaterialia*, 2012, **8**, 2360-2374.
19. X. Xia, C. Davies, J. Nie and N. Birbilis, *Corrosion*, 2014.
20. M. Bornapour, N. Muja, D. Shum-Tim, M. Cerruti and M. Pekguleryuz, *Acta biomaterialia*, 2013, **9**, 5319-5330.
21. M. Bornapour, M. Celikin, M. Cerruti and M. Pekguleryuz, *Materials Science and Engineering: C*, 2014, **35**, 267-282.
22. Y. Li, C. Wen, D. Mushahary, R. Sravanthi, N. Harishankar, G. Pande and P. Hodgson, *Acta biomaterialia*, 2012, **8**, 3177-3188.
23. N. T. Kirkland and N. Birbilis, *Magnesium Biomaterials: Design, Testing, and Best Practice*, Springer, 2014.
24. A. Standard, Designation ASTM G, 1992.
25. K. Anselme, *Biomaterials*, 2000, **21**, 667-681.
26. X. Chen, D. Nisbet, R. Li, P. Smith, T. Abbott, M. Easton, D.-H. Zhang and N. Birbilis, *Acta biomaterialia*, 2014, **10**, 1463-1474.
27. R. W. Li, N. T. Kirkland, J. Truong, J. Wang, P. N. Smith, N. Birbilis and D. R. Nisbet, *Journal of Biomedical Materials Research Part A*, 2014, **102**, 4346-4357.
28. A. C. Hänzi, I. Gerber, M. Schinhammer, J. F. Löffler and P. J. Uggowitzer, *Acta biomaterialia*, 2010, **6**, 1824-1833.
29. M. Schumacher, A. Lode, A. Helth and M. Gelinsky, *Acta biomaterialia*, 2013, **9**, 9547-9557.
30. A. A. Nayeb-Hashemi, J. B. Clark and A. S. M. International, *Phase diagrams of binary magnesium alloys*, ASM International, Metals Park, Ohio, 1988.
31. S. Jung, K. M. Panchalingam, L. Rosenberg and L. A. Behie, *Stem cells international*, 2012, **2012**.
32. N. Kirkland, N. Birbilis and M. Staiger, *Acta biomaterialia*, 2012, **8**, 925-936.

33. I. S. Berglund, H. S. Brar, N. Dolgova, A. P. Acharya, B. G. Keselowsky, M. Sarntinoranont and M. V. Manuel, *Journal of Biomedical Materials Research Part B: Applied Biomaterials*, 2012, **100**, 1524-1534.
34. X. Gu, Y. Zheng, Y. Cheng, S. Zhong and T. Xi, *Biomaterials*, 2009, **30**, 484-498.
35. J. Waterman, N. Birbilis, G. Dias, T. Woodfield and M. Staiger, *Corrosion Engineering, Science and Technology*, 2012, **47**, 340-345.
36. G. Williams, H. N. McMurray and R. Grace, *Electrochimica Acta*, 2010, **55**, 7824-7833.
37. J. H. Weiss, S. L. Sensi and J. Y. Koh, *Trends in Pharmacological Sciences*, 2000, **21**, 395-401.
38. G. J. Fosmire, *The American journal of clinical nutrition*, 1990, **51**, 225-227.
39. E. Canalis, M. Hott, P. Deloffre, Y. Tsouderos and P. Marie, *Bone*, 1996, **18**, 517-523.
40. T. Brennan, M. Rybchyn, W. Green, S. Atwa, A. Conigrave and R. Mason, *British journal of pharmacology*, 2009, **157**, 1291-1300.
41. G. Dagang, X. Kewei and H. Yong, *Journal of Biomedical Materials Research Part A*, 2008, **86**, 947-958.
42. M. Tian, F. Chen, W. Song, Y. Song, Y. Chen, C. Wan, X. Yu and X. Zhang, *Journal of Materials Science: Materials in Medicine*, 2009, **20**, 1505-1512.
43. K. Qiu, X. J. Zhao, C. X. Wan, C. S. Zhao and Y. W. Chen, *Biomaterials*, 2006, **27**, 1277-1286.
44. J.-W. Park, H.-K. Kim, Y.-J. Kim, J.-H. Jang, H. Song and T. Hanawa, *Acta biomaterialia*, 2010, **6**, 2843-2851.
45. D. Mushahary, R. Sravanthi, Y. Li, M. J. Kumar, N. Harishankar, P. D. Hodgson, C. Wen and G. Pande, *International journal of nanomedicine*, 2013, **8**, 2887.
46. M. Schumacher, A. Lode, A. Helth and M. Gelinsky, *Acta Biomaterialia*, 2013, **9**, 9547-9557.

Table 1. Nominal and chemical compositions (wt.%) of Mg alloys.

Alloy	Chemical composition (wt.%)					
	Mg	Sr	Zn	Fe	C	Mn
Mg-0.05Sr	Balance	0.040	0.007	0.008	0.030	0.015
Mg-0.1Sr	Balance	0.085	0.004	0.013	0.020	0.015
Mg-0.2Sr	Balance	0.167	0.004	0.015	0.020	0.011
Mg-0.5Zn-0.05Sr	Balance	0.041	0.460	0.006	0.020	-
Mg-1Zn-0.05Sr	Balance	0.044	1.020	0.007	0.020	-
Mg-1Zn-0.1Sr	Balance	0.096	1.030	0.006	0.020	-

Table 2. Compositions of human plasma and MEM medium (unit: mmol l^{-1}).

Compositions	Human plasma	MEM
Na^{+}	142	117.4
Cl^{-}	103	123.5
K^{+}	5.0	5.4
Ca^{2+}	2.5	1.8
Mg^{2+}	1.5	0.4
HPO_4^{2-}	1.0	1.0
SO_4^{2-}	0.5	0.4
D-Glucose	5	5.5
Bicarbonate (HCO^{3-})	22-30	26.2
Phenol red	-	0.03
Albumin (g l^{-1})	34-54	-

Table 3. Corrosion rates estimated by electrochemical and immersion tests of pure Mg control, binary Mg-Sr and ternary Mg-Zn-Sr alloys in MEM at 37 °C.

Material	Corrosion potential, E (V_{SCE})	Corrosion current density, i ($\mu A\ cm^{-2}$)	Immersion corrosion rate (mg day^{-1} cm^{-2})			
			1 day	3 days	7 days	14 days
Pure Mg	-1.62±0.05	32.5±2.6	0.62±0.04	1.55±0.07	2.06 ± 0.11	2.27±0.13
Mg-0.05Sr	-1.67±0.05	20.1±3.0	0.76±0.04	1.47±0.04	2.11±0.02	2.16±0.01
Mg-0.1Sr	-1.68±0.01	23.2±0.2	0.78±0.05	1.40±0.09	2.07±0.10	2.09±0.05
Mg-0.2Sr	-1.67±0.02	19.8±2.2	0.71±0.09	1.28±0.06	2.09±0.11	2.06±0.06
Mg-0.5Zn-0.05Sr	-1.66±0.01	11.0±2.6	0.80±0.07	1.51±0.09	2.10±0.14	2.09±0.12
Mg-1Zn-0.05Sr	-1.63±0.03	6.5±0.5	0.78±0.08	1.46±0.04	2.10±0.09	2.12±0.07
Mg-1Zn-0.1Sr	-1.67±0.01	8.7±1.7	0.78±0.08	1.64±0.07	2.14±0.15	1.80±0.07

Table 4. Mg, Sr and Zn ion concentrations (M) of different alloy extracts after immersing in DMEM solution at 37°C for 2 and 10 h, derived from determining the mass of alloys dissolved in DMEM under the same conditions.

Immersion time	Alloys	$[Mg^{2+}](M)$	$[Sr^{2+}](M)$	$[Zn^{2+}](M)$
2 h	Mg-0.05Sr	1.64×10^{-2}	1.83×10^{-6}	-
	Mg-0.1Sr	1.03×10^{-2}	2.43×10^{-6}	-
	Mg-0.2Sr	1.03×10^{-2}	4.77×10^{-6}	-
	Mg-0.5Zn-0.05Sr	1.02×10^{-2}	1.17×10^{-6}	1.76×10^{-5}
	Mg-1Zn-0.05Sr	1.02×10^{-2}	1.26×10^{-6}	3.90×10^{-5}
	Mg-1Zn-0.1Sr	1.02×10^{-2}	2.74×10^{-6}	3.94×10^{-5}
10 h	Mg-0.05Sr	2.67×10^{-2}	2.97×10^{-6}	-
	Mg-0.1Sr	1.85×10^{-2}	4.37×10^{-6}	-
	Mg-0.2Sr	1.85×10^{-2}	8.58×10^{-6}	-
	Mg-0.5Zn-0.05Sr	1.84×10^{-2}	2.11×10^{-6}	3.17×10^{-5}
	Mg-1Zn-0.05Sr	1.83×10^{-2}	2.26×10^{-6}	7.02×10^{-5}
	Mg-1Zn-0.1Sr	1.63×10^{-2}	4.38×10^{-6}	6.30×10^{-5}

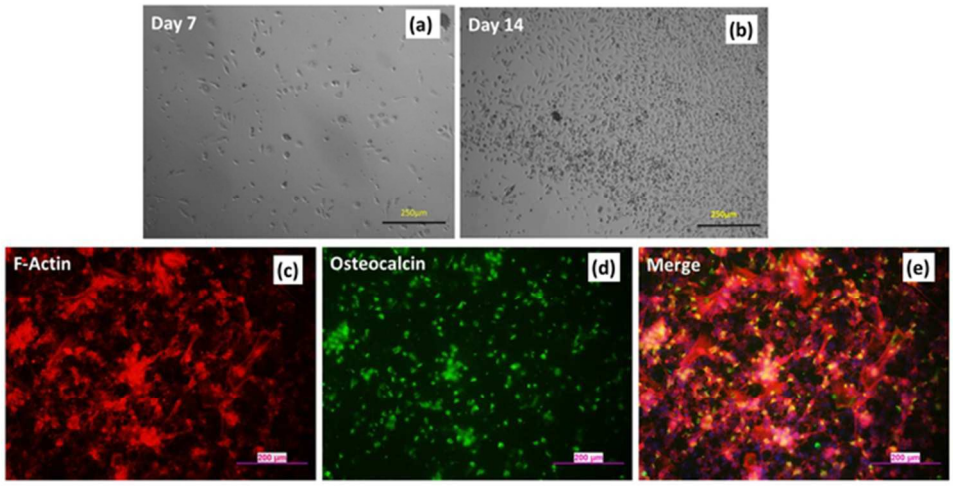

Figure 1. Isolated primary mouse osteoblasts cultured on cell culture plates for (a) 7 d and (b) 14 d; (c) F-Actin, (d) osteocalcin detected in 14 d osteoblastic culture and (e) merged image of (c) and (d).
59x29mm (300 x 300 DPI)

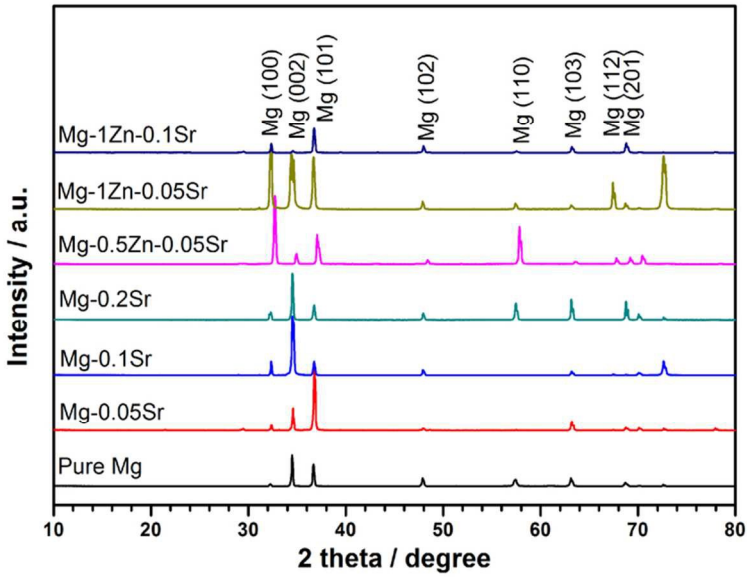

Figure 2. Respective X-ray diffraction patterns of pure Mg control, Mg-0.05Sr, Mg-0.1Sr, Mg-0.2Sr, Mg-0.5Zn-0.05Sr, Mg-1Zn-0.05Sr and Mg-1Zn-0.1Sr (wt.%).
83x58mm (300 x 300 DPI)

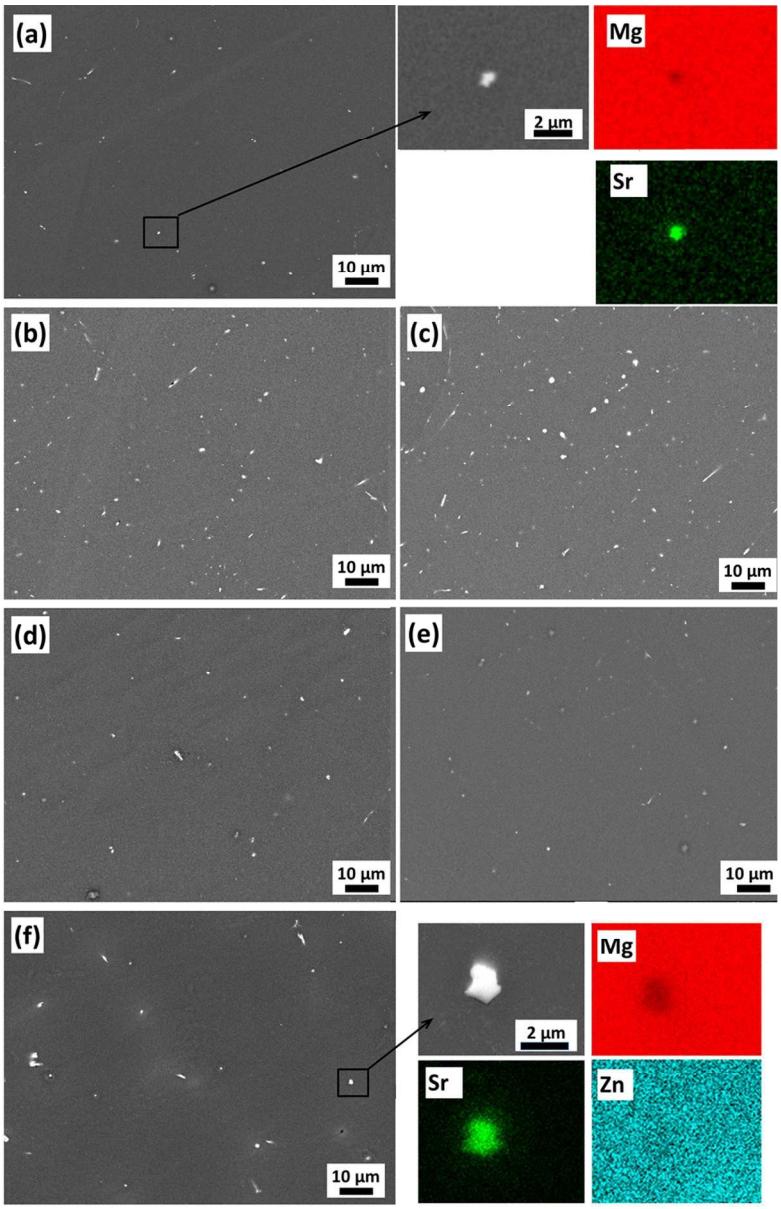

Figure 3. Backscattered electron SEM images and EDX mapping of (a) Mg-0.05Sr, (b) Mg-0.1Sr, (c) Mg-0.2Sr, (d) Mg-0.5Zn-0.05Sr, (e) Mg-1Zn-0.05Sr and (f) Mg-1Zn-0.1Sr.
184x282mm (300 x 300 DPI)

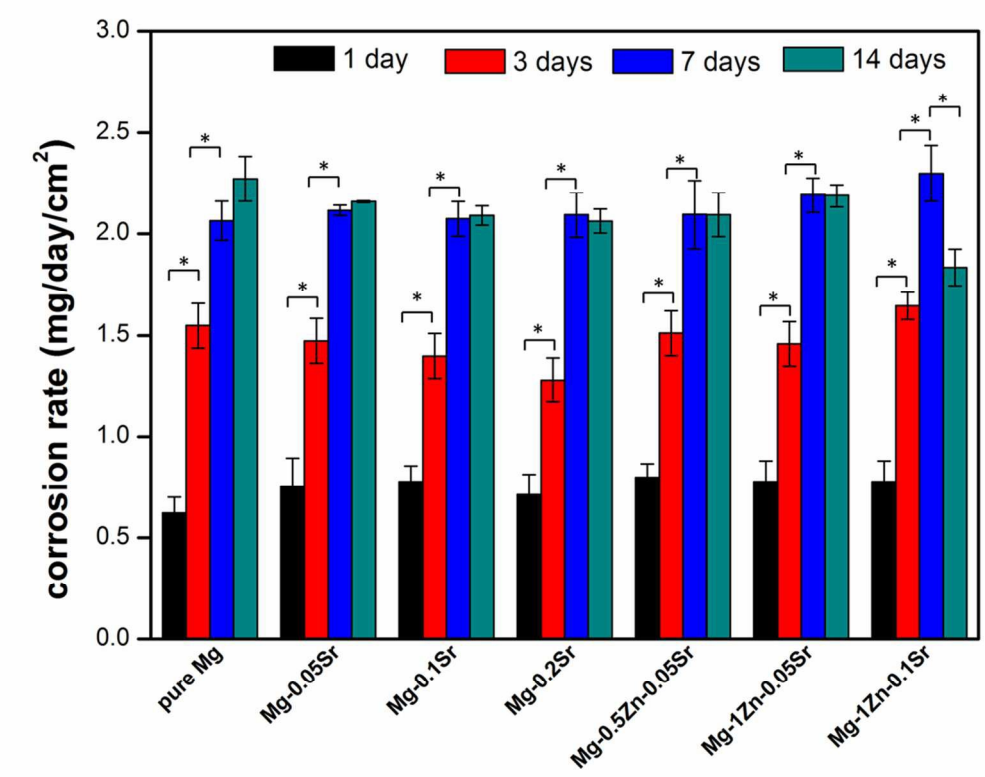

Figure 4. Mean corrosion rate is displayed in the form of mass loss with a unit of mg day-1 cm-2, derived from immersion testing of various Mg samples in MEM at 37 °C over defined time durations of 1, 3, 7 and 14 days, respectively, revealing no significant influence of addition of micro-level Sr on the general corrosion rate of Mg in MEM. (Error bar represents standard deviations and differences at *p < 0.05 are considered statistically significant.)
93x72mm (300 x 300 DPI)

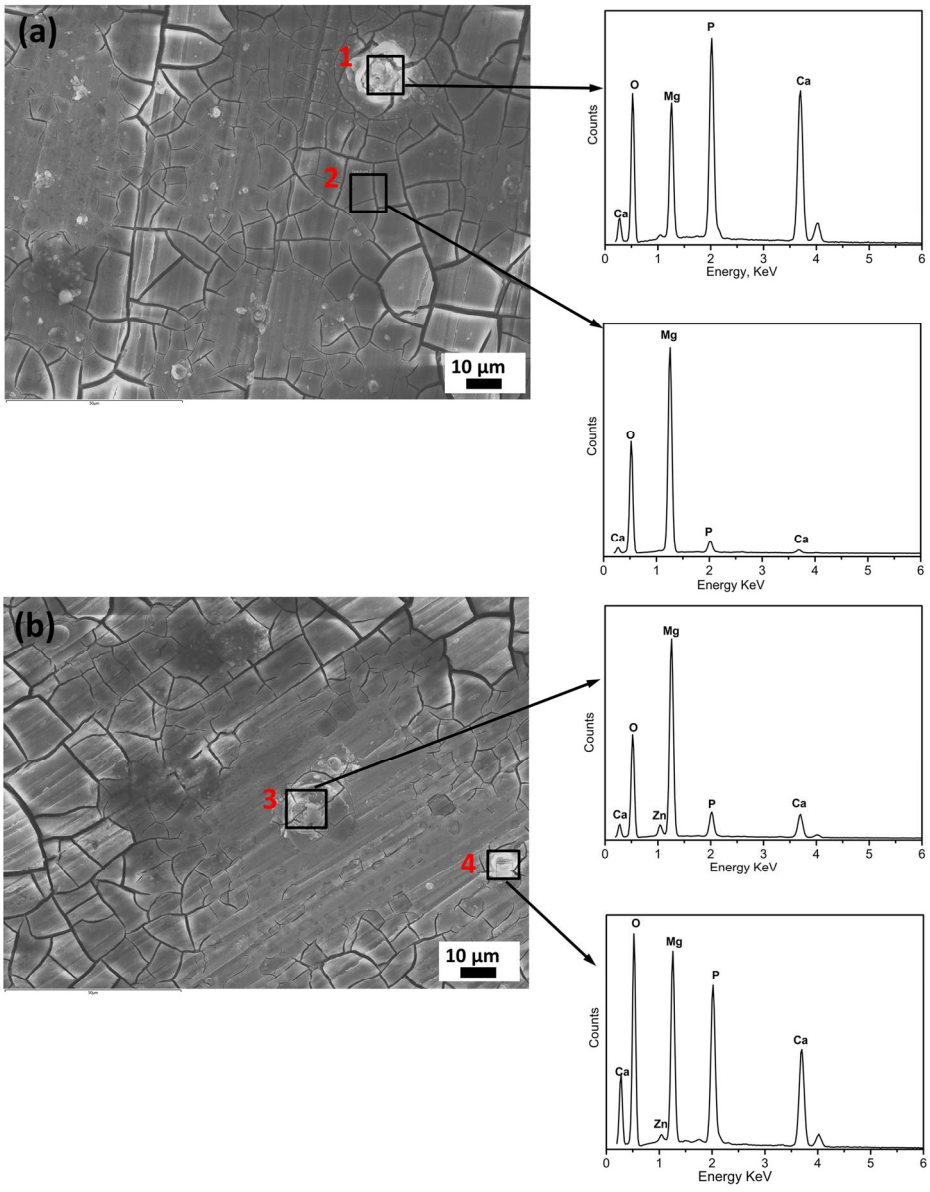

Figure 5. Secondary electron SEM images and corresponding EDX analysis at characteristic regions as denoted by arrows. Specimens represent (a) Mg-0.1Sr and (b) Mg-1Zn-0.05Sr after immersion in MEM for 24 h at 37 °C.
154x198mm (300 x 300 DPI)

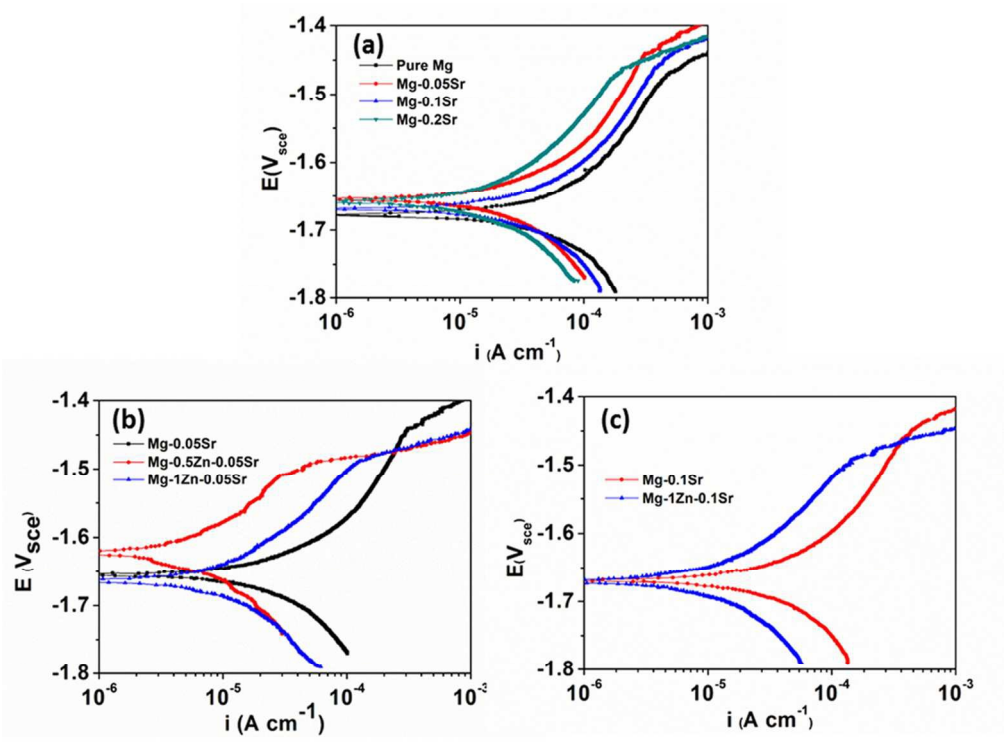

Figure 6. Potentiodynamic polarisation curves of pure Mg, binary Mg-Sr and ternary Mg-Zn-Sr alloys in MEM tested at 37°C.
90x68mm (300 x 300 DPI)

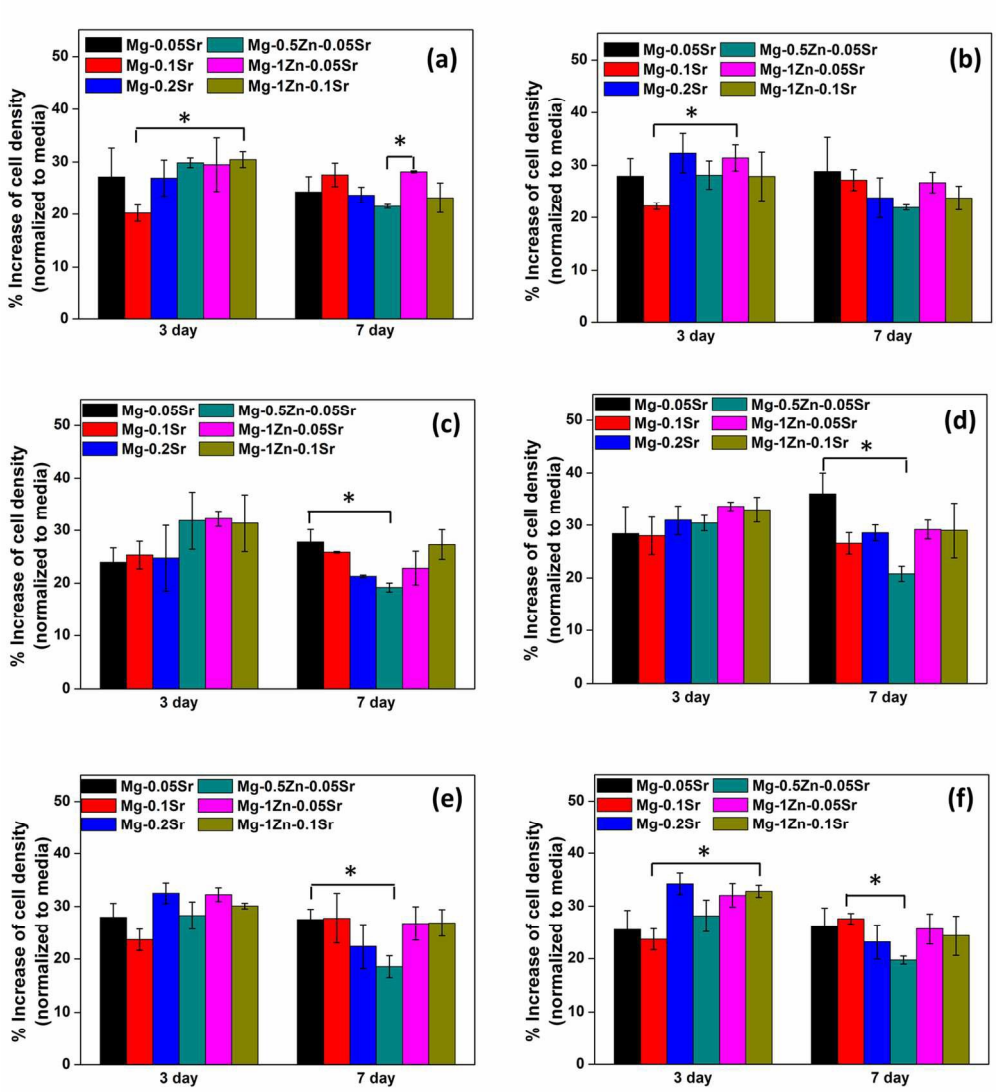

Figure 7. Effects of the degradation extracts on primary mouse osteoblasts were analysed by MTT proliferation assay. The cell viability after exposed to different concentrations (0.1%, 1% and 10%) of the 2 h and 10 h degradation extracts of Mg-0.05Sr, Mg-0.1Sr, Mg-0.2Sr, Mg-0.5Zn-0.05Sr, Mg-1Zn-0.5Sr and Mg-1Zn-0.1Sr was determined on day 3 (black) and day 7 (red) and presented as a percentage increase (or decrease) compared to the control: cells were exposed to (a) 2 h extracts at concentration of 0.1% (b) 2 h extracts at concentration of 1% (c) 2 h extracts at concentration of 10% (d) 10 h extracts at concentration of 0.1% (e) 10 h extracts at concentration of 1% (f) 10 h extracts at concentration of 10%. (Error bar represents standard deviations and differences at *p < 0.05 are considered statistically significant.)
135x154mm (300 x 300 DPI)

Graphical Abstract:

Alloying of micro levels of Sr do not promote the *in vitro* cathodic reaction whilst slightly moderating anodic kinetic upon Mg in MEM (a), and adopted micro additions of Sr around its solid solubility in Mg implant were favourable for bone growth (b).